77th IIW Annual Assembly and International Conference on Welding and Joining 7-12 July 2024 Rhodes, Greece

Compared to weld zone by Welding method to Cryogenic Austenitic Stainless Steel

JaeHan Park[1,2], *JeongYeol Park*[1], and *ChangYook Ji*[1*]

[1]Ulsan regional division Smart Forming Process Group, Ulsan, South Korea
[2]Pusan National University Materials Science and Engineering, Busan, South Korea

Abstract. The International Maritime Organization (IMO) has implemented regulations since 2020 to strengthen the sulfur content of ship fuels from 3.5% to 0.5%. However, in use Liquefied Natural Gas(LNG) primarily consists of liquefied methane, which emits methane during production, transportation, and distribution processes. To significantly reduce greenhouse gases such as carbon monoxide, carbon dioxide, and methane, hydrogen energy is gaining attention as an alternative fuel. Compared with fossil fuels, hydrogen has sufficient economic viability in terms of production, transportation, storage, and versatility. Liquid hydrogen, in particular, has the advantage of significantly reducing volume by 1/800 compared to gaseous hydrogen, leading to about a 7 times increase in efficiency in storage and transportation, without the need for a separate dehydrogenation process. Therefore, it is a pivotal moment for the technological development of transportation methods that can utilize liquefied hydrogen in either gaseous or liquid states. In this study, GTAW (Gas Tungsten Arc Welding) and GMAW (Gas Metal Arc Welding) were performed using austenitic stainless steel. To compare the processes, differences in tensile strength and V-charpy impact strength values were analyzed used OM (Optical Microscopy) and EBSD (Electron Backscatter Diffraction) for understanding the causes of mechanical property differences.

1. Introduction

The Kyoto Protocol established greenhouse gas reduction obligations for developed countries during the 2008-2020 period. However, a combination of developed countries refusing to shoulder the burden and a sharp increase in greenhouse gas emissions from developing countries led to a significant rise in emissions, exacerbating the climate crisis. To address this, the Paris Agreement, applicable to all countries from 2020 onwards, was adopted[1]. The International Maritime Organization (IMO) introduced the Global Sulfur Cap 2020, which mandates that all ships engaged in international voyages must use fuel oil with a sulfur content of no more than 0.5% (m/m) to reduce sulfur oxides (SOx), a significant air pollutant from ships[2].
LNG, a popular eco-friendly fuel, contains very low sulfur levels and can comply with IMO's sulfur content regulations. However, LNG's primary component is liquefied methane, which poses limitations for future IMO regulations[3]. As an alternative fuel to significantly reduce greenhouse gases like CO, CO2, and CH4, hydrogen energy is gaining attention. Liquid hydrogen, in particular, offers economic advantages due to its reduced volume—1/800 of its gaseous state—which improves storage and transportation efficiency by about seven times.[4]
There is active development of ships powered by eco-friendly fuels that emit fewer greenhouse gases compared to LNG-powered ships. Although various alternatives such as biogas, ammonia, and hydrogen have emerged, liquefied hydrogen stands out for its transportation and economic feasibility. The safety standards development plans for hydrogen fuel proposed by the Maritime Safety Committee and Norwegian Classification Society are largely based on ISO/TR 15916 (Basic considerations for the safety of ships using hydrogen as fuel). Literature indicates that materials and welds must maintain structural integrity in cryogenic (20K) and hydrogen environments[5].
Various candidates for manufacturing hydrogen tanks include aluminum alloys, titanium alloys, nickel steel, and high manganese steel, but austenitic stainless steel is the most promising. Due to its FCC structure, austenitic stainless steel has slower hydrogen diffusion and smaller segregation, requiring 10-100 times more hydrogen to cause hydrogen embrittlement compared to BCC metals[6]. AISI 304L, an austenitic stainless steel, is widely used in environments prone to corrosion for storage tanks and valves, and has been reported to be used in the liquefied hydrogen carrier Suiso Frontier by Kawasaki Heavy Industries, indicating its reliability for liquefied hydrogen tanks.
Previous studies have compared GMAW and GTAW processes using 304L and 316L, noting differences in mechanical properties due to cooling rate differences affecting δ-Ferrite proportions[7]. However, these studies mainly used optical microscopy for microstructure observation and lacked detailed microstructural analysis. While there are reports comparing GMAW and GTAW processes with varying shielding gases and current values, these also primarily focused on mechanical properties[8]. This study aims to establish fundamental data by analyzing the mechanical properties and microstructure differences between GTAW and GMAW welding processes using 304L.

* Corresponding author: cwji@kitech.re.kr

2. Experimental method

The specimens used in this study were 2mm thick plates of Austenitic Stainless Steel 304L, sized 150×50mm, with 1.2mm Filler Wire 308L. The relevant material properties are listed in Table 1.

		C ≤	Si ≤	Mn ≤	P ≤	S ≤	Cr	Ni
Base metal	SUS304L	0.03	1.00	2.00	0.045	0.030	18.00–20.00	9.00–13.00
Filler wire	SUS308L	0.02–0.03	0.30–0.65	1.00–2.500	0.03	0.03	19.55–22.0	9.0–11.00

Table 1. Material properties to Base metal and Filler wire

For GMAW, a Fronius VR 7000CMT welder with a KUKA robotic system was used, while for GTAW, a Fronius MW2200 welder with a Hyundai Engineering robotic system was used(Fig. 1.). The welding conditions were set for butt welding with GMAW at a current of 150A and a welding speed of 70cpm, and GTAW at a current of 250A and a speed of 40cpm. The shielding gases used were Ar 80% CO_2 20% for GMAW and pure Ar for GTAW. The tensile test specimens were prepared according to ASTM E 8/E 8M-08 standards and the impact test specimens were prepared according to ASTM E23-07 standards(Fig. 2.). Macro, OM, SEM, and EBSD were used to analyze the physical differences in the weld zones.

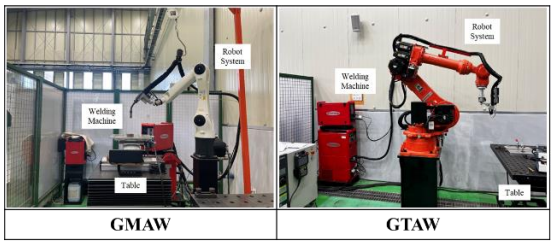

Fig. 1. Photos of GMAW and GTAW Weld robotic system

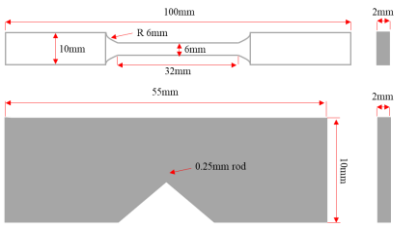

Fig. 2. Deisgn for Tensile Strength test and Charpy impact test specimen.

3. Results

3.1 Tensile Strength & Hardness

Tensile strength tests at room temperature were performed five times per welding process. The GMAW weld zone showed an average tensile strength of 711.04 MPa and an average elongation of 24.846%, while the GTAW weld zone showed an average tensile strength of 771.376 MPa and an average elongation of 39.132%. Thus, GTAW had a tensile strength 60.336 MPa higher and an elongation 14.286% greater than GMAW(Fig. 3.).

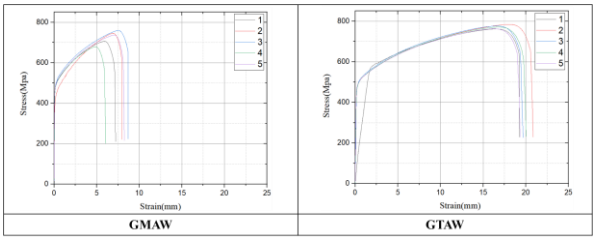

Fig. 3. Tensile test graph of GMAW and GTAW weld zone

All tensile tests showed fractures occurring in the weld zones. Hardness measurements were conducted to verify trends, showing an average hardness of 193.35 HV for GMAW welds, 198.45 HV for GTAW welds, and 199.42 HV for the base material(Fig. 4.).

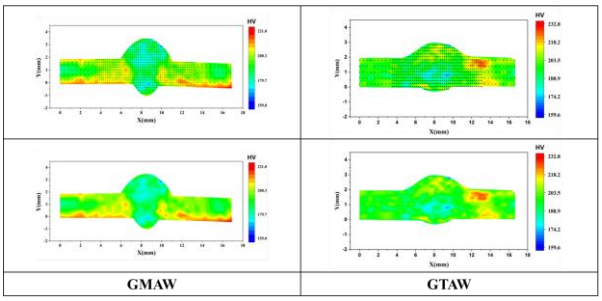

Fig. 4. Hardness mapping of GMAW and GTAW weld zones shows that the base metal hardness is generally higher than the fusion zone hardness.

3.2 Weld zone cross-section Microstructure

Observation of GMAW and GTAW weld zones through OM and SEM revealed that the GMAW weld zone formed a skeletal ferritic network (vermicular) at the dendritic grain boundaries, while the GTAW weld zone formed lathy ferrite structures. This is believed to be due to the differences in heat input between the processes. EBSD analysis to determine δ-Ferrite proportions showed 1.79% for GMAW and 2.14% for GTAW, with GTAW having a 0.35% higher δ-Ferrite proportions(Fig. 5.). EDS(Energy Dispersive Spectroscopy) analysis indicated a higher Ni content in the GMAW weld zone compared to the GTAW weld zone, possibly due to the closer distance between the base material and fusion zone in GTAW.

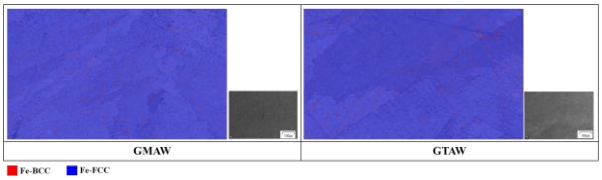

Fig. 5. EBSD image the GMAW and GTAW weld zone. Red color indicates δ-Ferrite. Blue color indicates γ-Austenitie.

3.3 V-Charpy Impact Test

V-Charpy impact tests were conducted to evaluate the physical properties of the weld zones, with three tests

performed per welding process. At room temperature, GMAW exhibited 16J and GTAW exhibited 22J, while at 77K, GMAW showed 19J and GTAW showed 27J. EBSD analysis of the 77K impact test specimens revealed that GTAW experienced transformation (γ-Austenite to ε-Martensite to α-Martensite) due to reduced stacking fault energy (SFE) during cryogenic impact test(Fig. 6.)[9]. The higher Ni content in the GMAW weld zone resulted in relatively higher SFE[10], preventing martensitic transformation and resulting in lower impact strength compared to GTAW.

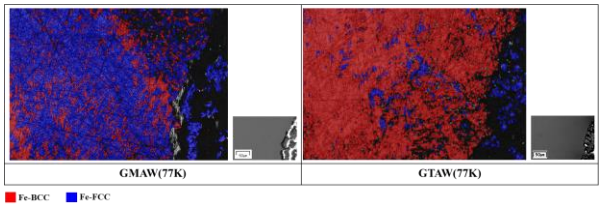

Fig. 6. EBSD image the Impact test part of GMAW and GTAW weld zone. Red color indicates δ-Ferrite. Blue color indicates γ-Austenitie. Additionally, Detecting the yellow color indicates the presence of ε-martensite.

4. Conclusion

For STS304L weld zones, GTAW exhibited superior mechanical properties compared to GMAW in single-pass welding. This superiority is attributed to differences in heat input and Ni content control affecting SFE. The Charpy impact test indicated limitations in evaluating fracture toughness at temperatures below 77K. The potential to control the low SFE characteristic of austenitic stainless steel through property adjustments was confirmed.

5. Reference

1. McKay, D.I.A.; Staal, A.; Abrams, J.F.; Winkelmann, R.; Sakschewski, B.; Loriani, S.; Fetzer, I.; Cornell, S.E.; Rockström, J.; Lenton, T.M. Exceeding 1.5°C Global Warming Could Trigger Multiple Climate Tipping Points. *Science (80-.).* **2022**, *377*, doi:10.1126/science.abn7950.
2. Islam, A.; Teo, S.H.; Ng, C.H.; Taufiq-Yap, Y.H.; Choong, S.Y.T.; Awual, M.R. Progress in Recent Sustainable Materials for Greenhouse Gas (NOx and SOx) Emission Mitigation. *Prog. Mater. Sci.* **2023**, *132*, 101033, doi:10.1016/j.pmatsci.2022.101033.
3. Gronholm, T.; Makela, T.; Hatakka, J.; Jalkanen, J.P.; Kuula, J.; Laurila, T.; Laakso, L.; Kukkonen, J. Evaluation of Methane Emissions Originating from LNG Ships Based on the Measurements at a Remote Marine Station. *Environ. Sci. Technol.* **2021**, *55*, 13677–13686, doi:10.1021/acs.est.1c03293.
4. Lee, H.-J.; Park, E.-D. Research Trends in Ammonia Decomposition Catalysts for H_2 Synthesis. *J. Energy Eng.* **2021**, *30*, 8–19, doi:10.5855/energy.2021.30.2.008.
5. Aasadnia, M.; Mehrpooya, M. Large-Scale Liquid Hydrogen Production Methods and Approaches: A Review. *Appl. Energy* **2018**, *212*, 57–83, doi:10.1016/j.apenergy.2017.12.033.
6. Suzuki, T.; Shiota, K.; Izato, Y. ichiro; Komori, M.; Sato, K.; Takai, Y.; Ninomiya, T.; Miyake, A. Quantitative Risk Assessment Using a Japanese Hydrogen Refueling Station Model. *Int. J. Hydrogen Energy* **2021**, *46*, 8329–8343, doi:10.1016/j.ijhydene.2020.12.035.
7. Desu, R.K.; Nitin Krishnamurthy, H.; Balu, A.; Gupta, A.K.; Singh, S.K. Mechanical Properties of Austenitic Stainless Steel 304L and 316L at Elevated Temperatures. *J. Mater. Res. Technol.* **2016**, *5*, 13–20, doi:10.1016/j.jmrt.2015.04.001.
8. Satheesh Kumar, K. V.; Gejendhiran, S.; Prasath, M. Comparative Investigation of Mechanical Properties in GMAW/GTAW for Various Shielding Gas Compositions. *Mater. Manuf. Process.* **2014**, *29*, 996–1003, doi:10.1080/10426914.2014.901527.
9. Zheng, C.; Yu, W. Effect of Low-Temperature on Mechanical Behavior for an AISI 304 Austenitic Stainless Steel. *Mater. Sci. Eng. A* **2018**, *710*, 359–365, doi:10.1016/j.msea.2017.11.003.
10. Umemoto, M.; Owen, W.S. Effects of Austenitizing Temperature and Austenite Grain Size on the Formation of Athermal Martensite in an Iron-Nickel and an Iron-Nickel-Carbon Alloy. *Metall. Trans.* **1974**, *5*, 2041–2046.